ACS OMEGA

http://pubs.acs.org/journal/acsodf

Article

# Role of $SnO_2$ Nanoparticles for a Self-Forming Barrier Layer on a Mild Steel Surface in Hydrochloric Acid Medium Containing *Piper betle* Leaf Extract

Lai Xuan Bach, Thi-Bich-Ngoc Dao, Trung T. Pham, Robert Sporken, Thi Nhung Nguyen, S. V. Prabhakar Vattikuti,* Nhon Pham Van, and Nam Nguyen Dang*

Cite This: *ACS Omega* 2022, 7, 38061−38068

Read Online

ACCESS | Metrics & More | Article Recommendations | Supporting Information

**ABSTRACT:** The self-formation of a porous organic thin-film via corrosion inhibitor supports wide applications of carbon steel in industry. Unfortunately, serious damages could be concentrated to the pinhole and/or pore locations in the porous organic film, resulting in the localized corrosion even when an optimal concentration of organic corrosion inhibitors is used. In this work, $SnO_2$ nanoparticles are used for producing the more robust barrier layer via the self-migration of nanoparticles, resulting in a higher corrosion resistance, smooth and uniform protective layer, as well as the existence of $SnO_2$ in the protective layer that could directly affect the high inhibition performance. Therefore, the work suggests a new way to make a more robust thin film that could extend the use of organic corrosion inhibitors.

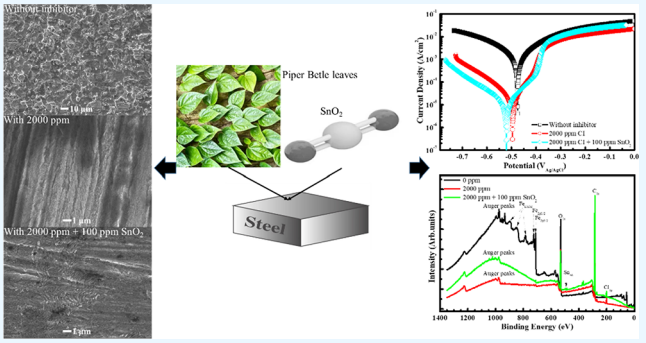


## 1. INTRODUCTION

Corrosion inhibitors can be categorized by how they protect the intended metal: cathodic type which deals with reactions in the environment, anodic type which deals with reactions on the metal, and mixed type which deals with both.[1] Nevertheless, it is more intuitive to group inhibitors according to their nature because it is very common to compare any given inhibitor to the strongest inhibitor group: the chromate-based inhibitors or chromates for short. Last but not least, the plant extracts are a combination of phytochemicals among which some chemicals have the desired corrosion inhibition effect.[2−5] However, because they are usually a bulk extract with multiple components, it is not easy to determine which components are useful for the purpose of ameliorating a particular corrosion problem under investigation.

One such investigation is the study of *Piper betle* leaf extract (PBLE) as a corrosion inhibitor for mild steel in hydrochloric acid[6,7] which has found moderate success in creating a reasonably well-performing film to alleviate the expected corrosion in the mentioned environment. Nonetheless, the resulting film was found to be porous, which was also predicted. One strategy to act on a porous film is to use nanoparticles (NPs) in conjunction with the inhibitor. Here, the proposed NP is tin oxide for several reasons. First and foremost, NP addition could be beneficial due the high surface area typical of this material, suitable for diffusing into the porous organic film (good contact).[8] Furthermore, tin oxide has mixed cation valences and oxygen vacancy defects, which would enable coordination chemistry[9] with the organic film as well as the underlying metal. Finally, while silica (silicon and tin belong to the same group IV-A in the periodic table) and other oxides[10] have been considered for corrosion inhibitor studies, tin oxide has been largely under the radar of the same topic of study. Therefore, this study focused on the role of nano tin oxide being incorporated into the corrosion inhibition of mild steel in hydrochloric acid solution that contains the betle leaf extract.

## 2. EXPERIMENTAL PROCEDURES

*Piper betle* leaves were collected from Southern Vietnam and then cleaned and processed into a coarse powder which was fed into a Soxhlet system containing ethanol at 75 °C to extract the soluble components in the *Piper betle* leaf. Subsequently, the obtained solution was fed into a rotary evaporator to produce the PBLE. The functional groups of PBLE were singled out and named using gas chromatography−mass spectrometry (GC−MS). The characterization was performed twice to validate its reproducibility, once at 320 and again at

**Received:** August 28, 2022
**Accepted:** September 30, 2022
**Published:** October 12, 2022

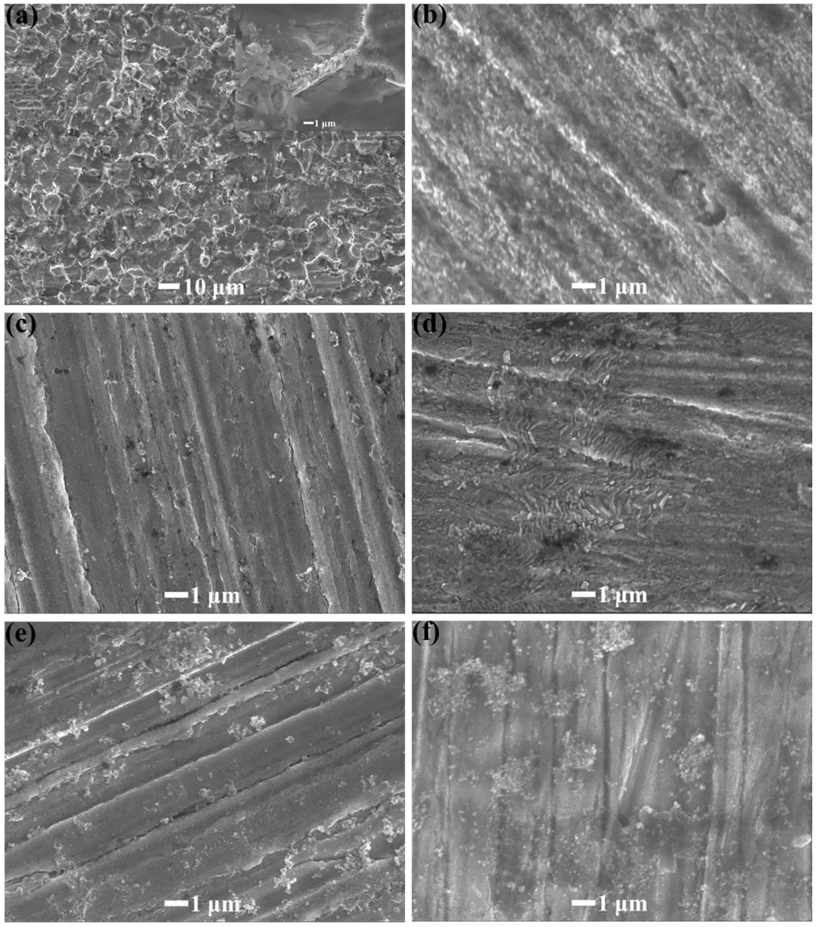


**Figure 1.** SEM images of mild steel surfaces after 24 h exposure to (a) 0.1 M HCl solution and 0.1 M HCl + 2000 ppm PBLE solutions with (b) 10, (c) 50, (d) 100, (e) 150, and (f) 200 ppm $SnO_2$ NP addition.

600 °C. Tin(IV) oxide nanopowder ($SnO_2$—CAS no. As 18282-10-5 and product no. As 549657-5G) with average particle size less than 100 nm was purchased from Sigma-Aldrich and directly used as a synergic addition to the corrosion inhibitor. 0, 10, 50, 100, 150, and 200 ppm $SnO_2$ was added to 0.1 M HCl solution (pH 1) containing 2000 ppm PBLE. First, the investigated 0.1 M HCl solution was prepared from the stock 37% HCl which would be then used to dissolve the appropriate amount of the condensed extract (effectively 2 g/L of PBLE). Second, the solution was alternated between ultrasonication and stirring at 600 rpm every 10 min for at least 2 h to ensure good solubility. Finally, the electrolyte for each condition was obtained by adding the respective quantity of the nanopowder into the above solution and similarly alternating between stirring and ultrasonication again for 40 min to achieve good dispersity, readying for the following electrochemical measurements.

The steel specimens were made by computer numerical control to achieve a flat surface area of 1 $cm^2$ to be used for a double-jacketed 250 mL cell (flat cell) for all electrochemical measurements. Before each measurement, the steel surface was ground by 2000-grit silicon carbide paper in one direction so that the grinding marks are all nearly parallel to each other. The flat cell was filled with the prepared electrolyte, as described above, of 0.1 M hydrochloric acid containing PBLE corrosion inhibitor at 2000 ppm concentration and $SnO_2$ synergic addition at different concentrations of 0, 10, 50, 100, 150, and 200 ppm, all at room temperature. The electrochemical cell followed a standard three-electrode system with the working electrode performed by the steel specimen, the reference electrode achieved by silver/silver chloride in saturated potassium chloride, and the counter electrode fulfilled by two titanium meshes. These three electrodes were connected to and monitored by a VSP electrochemical system. The first measurements were electrochemical impedance spectroscopy (EIS) and linear polarization resistance (LPR) which were recorded once every hour for 24 h, including the first period of 1 h open-circuit potential (OCP). Furthermore, potentiodynamic polarizations (PDs) in duplicates were scheduled at the end of 24 h OCP for each electrolyte condition. The setting for EIS was 10 mV peak-to-peak amplitude of the sinusoidal pertubation signals and $10^5$ to 0.01 Hz of the frequency range. As for LPR, the potential range was $\pm 25$ $mV_{OCP}$ and the scan rate was 0.5976 V/h, which was also the scan rate for the PD measurements.

Surface characterization comprised, first, of SEM to determine the effect of the corrosion inhibitor (2000 ppm PBLE) and its synergic addition (0, 10, 50, 100, 150, and 200 ppm $SnO_2$) in the aggressive acid solution on the surface morphology of the steel specimens after the 24 h immersion. Second, the 100 ppm $SnO_2$ condition (with 2000 ppm PBLE in hydrochloric acid 0.1 M) was picked for atomic force microscopy (AFM) according to previous results. AFM was undertaken by a Bruker Multimode, with the signal-to-noise ratio calculated by dividing the average signal value by the average noise value. Finally, there was also X-ray photoelectron


https://doi.org/10.1021/acsomega.2c05545
ACS Omega 2022, 7, 38061−38068

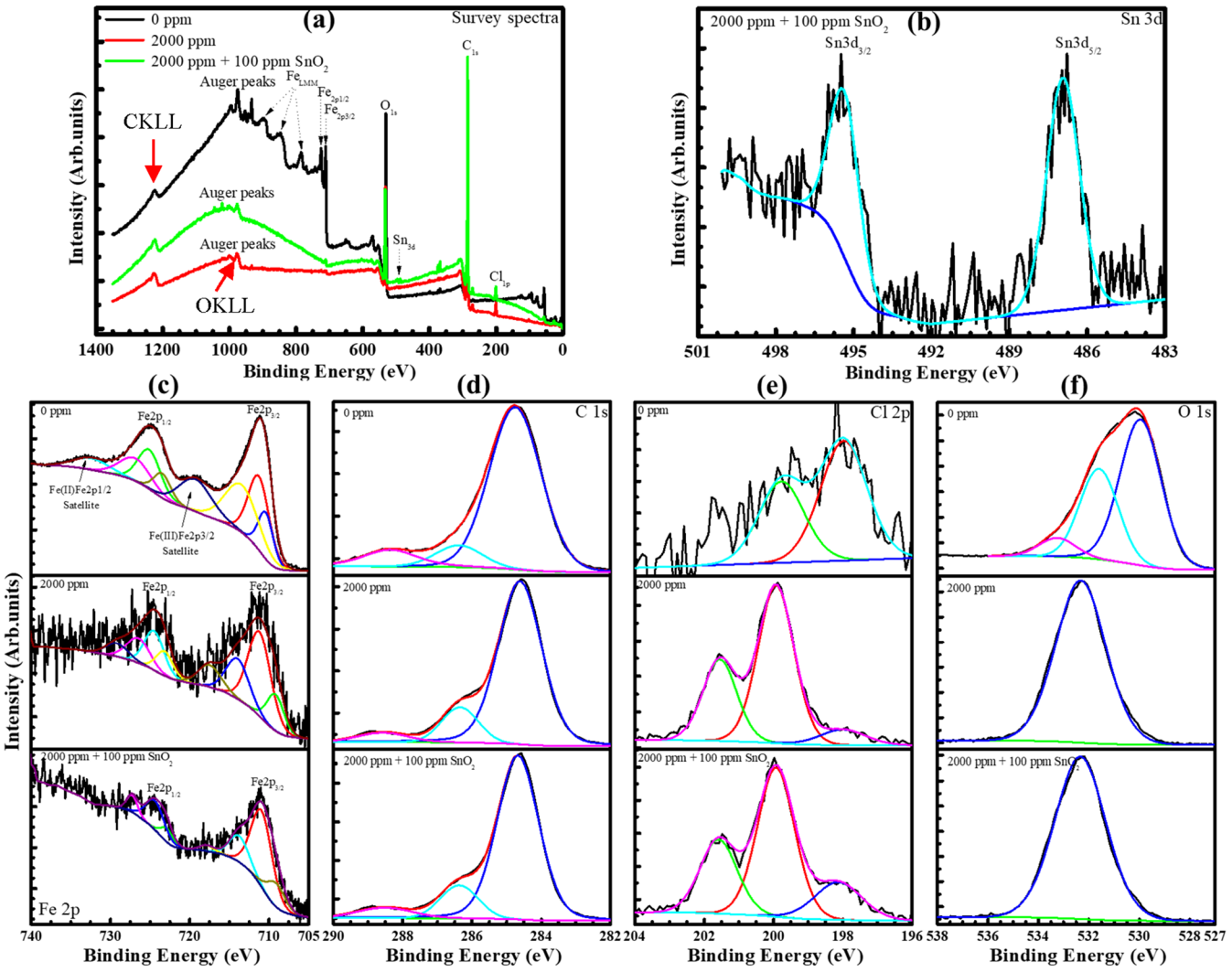


**Figure 2.** XPS spectra of mild steel surfaces after 24 h exposure to 0.1 M HCl solutions containing 0, 2000 ppm PBLE, and 2000 ppm PBLE + 100 ppm $SnO_2$: (a) Survey scan spectra and narrow scan spectra for (b) Sn 3d, (c) Fe 2p, (d) C 1s, (e) Cl 2p, and (f) O 1s.

spectroscopy (XPS, Kratos Nova) with an Al K$\alpha$ energy source at 1486.6 eV for steel specimens after 24 h OCP in these three conditions: 0 PBLE, 2000 ppm PBLE, and 2000 ppm PBLE + 100 ppm $SnO_2$.

## 3. RESULTS AND DISCUSSION

Figure 1a serves as a reminder to the susceptibility of mild steel in HCl 0.1 M, showing a severely degraded surface where parallel grinding marks have been rendered unrecognizable, unlike those in Figure S1a benefitting from the 2000 ppm PLBE corrosion inhibitor.[6] Because the corrosion inhibitor was kept at 2000 ppm for all NP additions, all following concentrations will refer to NP addition unless stated otherwise. The initial 10 ppm NP addition was actually detrimental to the surface integrity, as shown in Figure 1b. Up to 50 ppm, as in Figure 1c, was when the surface started to become much less porous, although pitting corrosion may still be present. The benefits of NP addition remained up to 100 ppm, visually from Figure 1d, after which there seemed to be clusters of NPs aggregated onto the surface at 150 and 200 ppm, as evident in Figure 1e,f. The AFM image in Figure S1b reaffirmed the performance of 2000 ppm PBLE corrosion inhibitor combined with 100 ppm $SnO_2$ NPs.

Figure 2 demonstrates three different XPS data from mild steel surfaces submerged in 0.1 M HCl for 24 h under three different conditions: without inhibitor, with inhibitor as it is, and with NP-incorporated inhibitor as given in the survey scan from Figure 2a. Figure 2c is indicative of complex corrosion products of the Fe $2p_{3/2}$ and Fe $2p_{1/2}$ peaks, close to the iron peaks of $Fe_2O_3$, FeO, and FeOOH described by Biesinger et al.[11] In addition, Fe(II)Fe $2p_{1/2}$ and Fe(III)Fe $2p_{3/2}$ satellites were observed only on the surface immersed in the solution without inhibitor addition. Furthermore, oxygen peaks in Figure 2f indicating oxides, hydroxides (of iron), and adsorbed water existed at 530, 532 and 533 eV, respectively. Besides, there was also a sign of metal (iron) carbide and carbonate from the 284.5 and 288 eV carbon peaks, respectively.[12] Finally, a negligible peak of metal chloride existed at 198 eV in the uninhibited surface which could point to one of FeOOH polymorphs.[13]

Figure 2d,e are remarkably similar in terms of positions and amplitudes of the carbon and chloride peaks of inhibited surfaces, which were dominated by organic contributions (200 and 201.5 eV peaks of organic chloride; 284.5, 286.4, and 289 eV of C−C, C−O, and O−C═O) rather than an inorganic one.[14] Moreover, the single oxygen peak at 532.5 eV could be


https://doi.org/10.1021/acsomega.2c05545
ACS Omega 2022, 7, 38061−38068

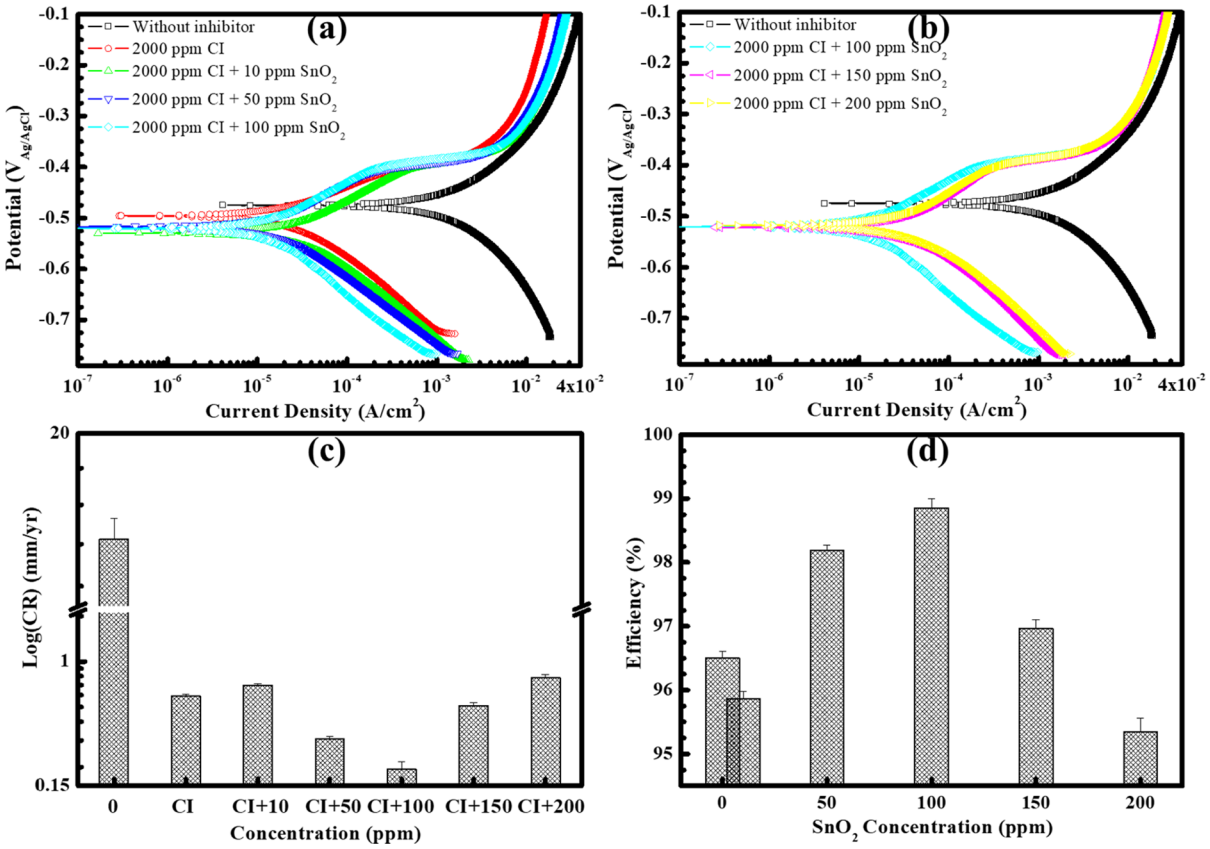


**Figure 3.** (a,b) Representation of PD results, (c) corrosion rate, and (d) inhibition efficiency of steel after 24 h exposure in a 0.1 M HCl solution without and with PBLE and $SnO_2$ NP addition.

**Table 1. Comparison of Corrosion Inhibition Efficiencies of Similar Published Works**

| refs | $\eta$ (%) | substrate | inhibitor (concentration) | corrosive |
|---|---|---|---|---|
| 18 | 95.7−97.6 | C1018 steel | $\alpha$-Al(OH)$_3$@AMTP (100 ppm) | 1.0 M $H_2SO_4$ |
| 19 | 95.3−98.8 | C1018 steel | $CoCrO_3$/polyaniline (150 ppm) | 0.1 M HCl + 3.5% NaCl |
| 20 | 94.1−97.8 | duplex steel | chitosan/Zn@$H_3$BTC (200 ppm) | 2.0 M $H_2SO_4$ |
| 21 | 88.1−98.6 | carbon steel | primary aminated modified cellulose/metal oxide NPs (250 ppm) | 1.0 M HCl |
| 22 | 98.20 | X60 steel | $CeO_2$@gelatin (5%) | 15% HCl at 50 °C |
| 23 | 98.18 | mild steel | graphene/$Fe_3O_4$@glycine (50 ppm) | 1.0 M HCl at 60 °C |
| 24 | 96.13−98.39 | carbon steel | magnetite NPs/polyvinyl pyrrolidone (0.1%) | 1.0 M HCl |
| 25 | 95.00 | mild steel | $TiO_2$ NPs/may flower extract (100 ppm) | well water |
| this work | 98.80 | mild steel | $SnO_2$ NPs/PBLE (2000 ppm) | 0.1 M HCl |

attributed to absorbed organic oxygen species,[15] distinguishable from the metal oxide peak of the uninhibited steel surface. Furthermore, this shift to higher binding energy could be explained by a higher covalence of the metal−oxygen bond where the electron density increased at the cost of the electron density on the oxygen ions.[16] However, the key difference lay in the fact that only one oxygen signal was found, meaning that the complicated iron oxides and hydroxides had been replaced with a single corrosion product which bonded with oxygen more covalently and was consequently more stable. These evidences combined with the significantly lowered intensities of iron signals (and the lack of iron Auger features) hinted at the prominence of a complete and unified protective layer on the mild steel surface as observed in the survey scan spectra in Figure 2a. Additionally, the presence of $SnO_2$ NPs in Figure 2b was confirmed around the 486.5 and 496 eV peaks.[17]

Figure 3 shows the PD of mild steel surfaces along with the corrosion rate and corrosion inhibition efficiency thereof. As with previous work,[6] there were both anodic and cathodic actions for the corrosion inhibitor, as shown in Figure 3a,b. NP additions were principally effective in the cathodic region, further shifting the cathodic branch to lower current densities (as well as lowering the corrosion potential). The shift in the corrosion potential was still within 100 mV of the result from the without-inhibitor condition, suggesting that anodic inhibition yet existed. The anodic part of the mixed inhibition, however, did not similarly receive all improvements. In fact, only 100 ppm was comparable to the base corrosion inhibitor without NPs, while other NP conditions suffered. Last but not least, the Tafel curves for inhibited systems exhibited an activation-controlled behavior with linear slopes on either cathodic and anodic branches,[18] enabling the use of extrapolation to obtain the corrosion rates and consequently corrosion inhibition efficiencies in Figure 3c,d. As expected from the above qualitative reasoning, 100 ppm did achieve the


https://doi.org/10.1021/acsomega.2c05545
ACS Omega 2022, 7, 38061−38068

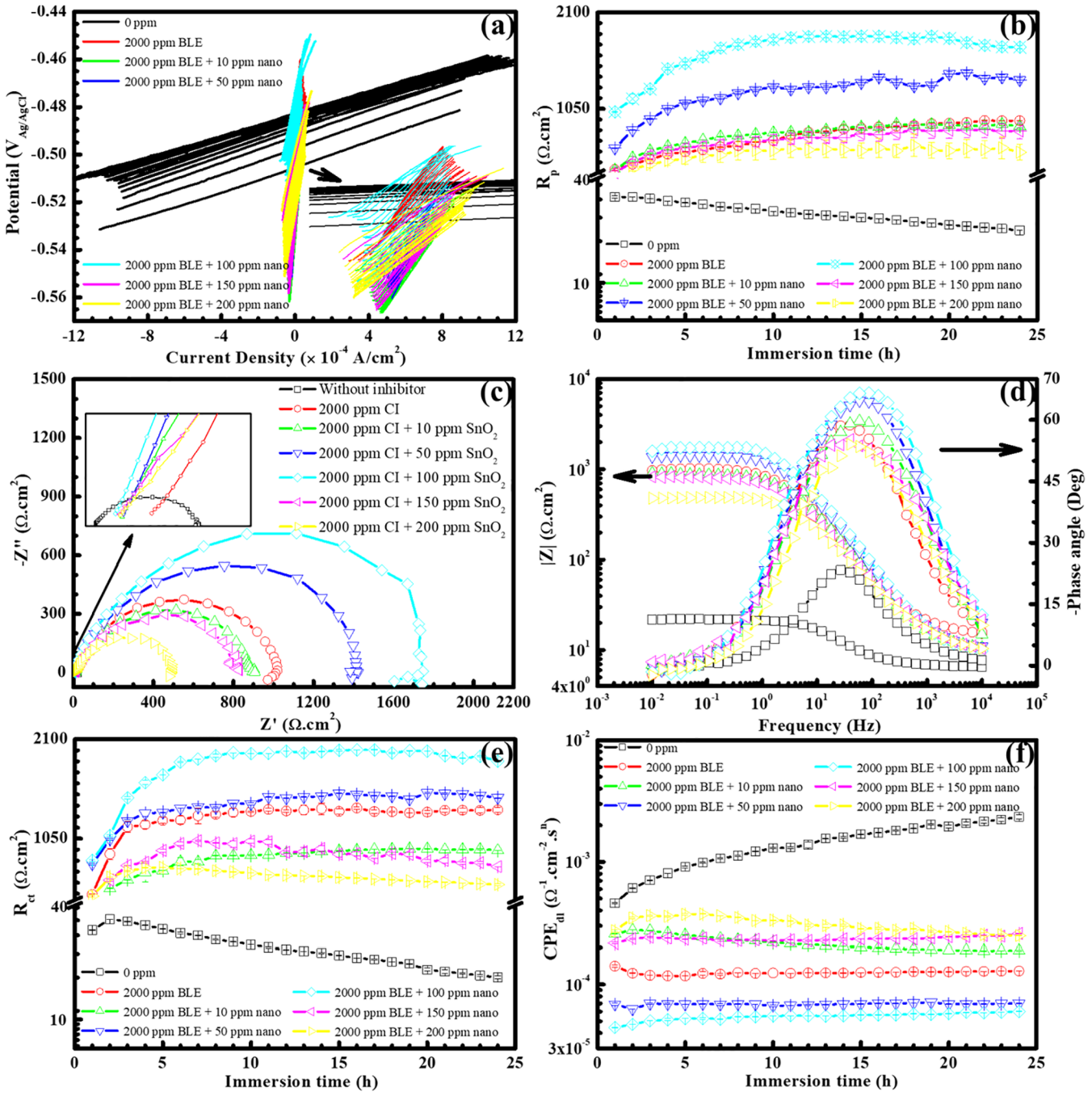


**Figure 4.** (a) LPR results during 24 h exposure of steel in the investigated solutions, (b) $R_p$ values observed by LPR measurements, (c,d) Nyquist and Bode plots of steel after 24 h exposure in the investigated solutions, (e,f) $R_p$ and double-layer CPE magnitude variation in time and concentrations observed by EIS measurements.

overall best performance which is also better than previous works in Table 1.

Evidence for the optimal NP concentration continued with the LPR results in Figure 4a,b, where 100 ppm achieved the highest $R_p$, followed by 50 and 0 ppm. It was noted that the polarization curves are largely linear which meant LPR was a suitable characterization technique for this situation (high enough corrosion rates). For EIS, all Nyquist semicircles for inhibited mild steel in Figure S2 grew with time (unlike uninhibited mild steel), and there were not many changes to their shape. In fact, all investigated NP conditions returned a similarly depressed shape, distinguishable mainly by their values, which were more clearly compared in Figure S3 with the impedance versus frequency Bode plots. However, there were substantial differences among the phase angle versus frequency Bode plots of Figure S4. As the NP concentration increased, the peak in the medium-frequency range steadily grew higher and wider, reaching a maximum at 100 ppm, after which its height was reduced to lower values than from before the NP addition. Figure 4c,d summarizes the Nyquist and Bode plots after 24 h of all investigated conditions.

From the obtained results, an equivalent circuit was proposed in Figure S5, where $R_s$ is the solution resistance, $C_{dl}$ (also referred to as $CPE_{dl}$) is the constant phase element of


https://doi.org/10.1021/acsomega.2c05545
ACS Omega 2022, 7, 38061−38068

the double layer, $R_p$ (also referred to as $R_{ct}$) is the charge-transfer resistance, and finally the inductive component $L$ and $R_L$ accounted for undefined adsorbed species.[26] Fitted results used in this circuit are presented in Figure 4e with $R_{ct}$ which resembled the experimental results in Figure 4b, and in Figure 4f with $CPE_{dl}$ which represented higher adhesion of protective film the lower it was. Once again, the superlative performance of 100 ppm has been reaffirmed, this time followed by those of 50 and 0 ppm. On a side note, it took longer for the fitted $R_p$ values of 100 ppm (8 h) to plateau compared with 50 and 0 ppm (4 h).

Figure S6 and Table S1 detail the components found in PBLE using GC−MS. The chief components are designated as having at least 50 quality, which are acetic acid, 2-methoxy-4-1-(1-propenyl), 2,5-dimethyl-, and 2-(2-pyridinyl)quinoline. When the corrosion inhibitor was initially introduced into the acidic solution, a strong interaction with the mild steel substrate was observed, drastically reducing the corrosion rate and the OCP (Figure S7). When the NPs were added to corrosion inhibitor formulation at a low concentration of 10 ppm, they induced changes in the electrical double layer at the steel surface, introducing a phenomenon similar to having an anodic inhibitor under its critical concentration and exaggerating localized corrosion. On the other hand, the benefit of NP addition can be explained from the Bode plots of Figure S4 where an improvement (in both height and width) for the medium-frequency range, which corresponded to the processes within the protective organic film (and its integrity), was found. This could indicate that the porous organic film had its pores filled, similar to what Hoai Vu et al. have achieved.[27] The first observation from XPS is the consolidated single corrosion product, similar to a passivated surface. The PD results can also confirm this with its obvious anodic passive region from −500 to −400 $mV_{Ag/AgCl}$. Furthermore, the strong XPS chloride peaks suggested that this aggressive ion has been fixed into the organic film, limiting its ability to accelerate corrosion of the protected steel.[6,14,28] Additionally, the lone oxygen peak also originated from the organic film as detailed in the XPS analysis above because 532.5 eV was too large to validate the existence of regular iron oxides and hydroxides. This furthered the benefits of PBLE as a corrosion inhibitor that strongly bonded with the mild steel substrate in 0.1 M HCl, preventing the formation of harmful corrosion products. Finally, while carbon and oxygen peaks underwent no recognizable changes after NP addition (especially at 100 ppm), iron peaks had a significant boost in amplitude, implying that the organic film probably became more compact after such NP addition. This is important because it is opposite to the regular fracturing volume increase of the natural oxidation of iron in the steel structure.

## 4. CONCLUSIONS

In conclusion, 100 ppm $SnO_2$ NP addition was successfully incorporated with PBLE corrosion inhibitor of mild steel in 0.1 M HCl such that the adsorbed PBLE organic film became denser and more compact while still conferring the desired passivation onto the steel surface in hydrochloric acid solution. The proposed mechanism involved the adsorbed PBLE main components competing against the formation of harmful corrosion products and the chloride ion fixation due to both the main and lesser components of PBLE. Furthermore, it was also shown that $SnO_2$ NP addition mainly affected the cathodic reactions and processes owing to the enhanced organic film's integrity, whereas the anodic counterpart did not improve. Overall, this has demonstrated that the combination of nanomaterial and corrosion inhibitor, particularly plant extract derivatives, is a promising approach to ameliorate electrochemical corrosion.

## ■ ASSOCIATED CONTENT

### Supporting Information

The Supporting Information is available free of charge at https://pubs.acs.org/doi/10.1021/acsomega.2c05545.

SEM images and AFM 2D image of the steel surface; EIS results in the form of Nyquist plots; EIS results in the form of Bode plots (impedance vs frequency); EIS results in the form of Bode plots (phase angle vs frequency); proposed equivalent circuit for fitting EIS data; GC−MS result of PBLE; and concentrations of the compounds detected by GC−MS (PDF)

## ■ AUTHOR INFORMATION


### Corresponding Authors

**S. V. Prabhakar Vattikuti** − *School of Mechanical Engineering, Yeungnam University, Gyeongsan 38541, Republic of Korea;* orcid.org/0000-0002-9009-5466; Email: drprabu@ynu.ac.kr

**Nam Nguyen Dang** − *Future Materials & Devices Laboratory, Institute of Fundamental and Applied Sciences, Duy Tan University, Ho Chi Minh City 700000, Vietnam; The Faculty of Environmental and Chemical Engineering, Duy Tan University, Da Nang 550000, Vietnam;* orcid.org/0000-0003-4434-0763; Email: nguyendangnam@duytan.edu.vn

### Authors

**Lai Xuan Bach** − *Future Materials & Devices Laboratory, Institute of Fundamental and Applied Sciences, Duy Tan University, Ho Chi Minh City 700000, Vietnam; The Faculty of Environmental and Chemical Engineering, Duy Tan University, Da Nang 550000, Vietnam;* orcid.org/0000-0002-9960-6218

**Thi-Bich-Ngoc Dao** − *Future Materials & Devices Laboratory, Institute of Fundamental and Applied Sciences, Duy Tan University, Ho Chi Minh City 700000, Vietnam; The Faculty of Environmental and Chemical Engineering, Duy Tan University, Da Nang 550000, Vietnam;* orcid.org/0000-0002-1410-3727

**Trung T. Pham** − *Namur Institute of Structured Matter (NISM), Department of Physics, University of Namur, Namur B-5000, Belgium*

**Robert Sporken** − *Namur Institute of Structured Matter (NISM), Department of Physics, University of Namur, Namur B-5000, Belgium;* orcid.org/0000-0002-4429-2039

**Thi Nhung Nguyen** − *Ho Chi Minh City University of Technology and Education, Ho Chi Minh City 700000, Vietnam*

**Nhon Pham Van** − *Nam Can Tho University, Can Tho City 94000, Vietnam*

Complete contact information is available at: https://pubs.acs.org/10.1021/acsomega.2c05545




https://doi.org/10.1021/acsomega.2c05545
ACS Omega 2022, 7, 38061−38068

### Author Contributions

L.X.B. and T.T.P. designed, conducted the experiment, and wrote the manuscript. T.-B.-N.D., T.N.N., and N.P.V. designed and conducted the synthesis. R.S., S.V.P.V., and N.N.D. partly designed, supervised the project, and corrected. All authors contributed to data analysis and approved the final version of the manuscript.

### Notes

The authors declare no competing financial interest.

## ■ ACKNOWLEDGMENTS

This work is sponsored by the NRF-Korea (2020R1A2B5B01002744).

## ■ ABBREVIATIONS

| | |
|---|---|
| PBLE | *Piper betle* leaf extract |
| NP | nanoparticle |
| $SnO_2$ | tin(IV) oxide |
| $\eta$ | corrosion inhibition efficiency |
| min | minute |
| rpm | revolutions per minute |
| HCl | hydrochloric acid |
| GC−MS | gas chromatography−mass spectroscopy |
| XPS | X-ray photoelectron spectroscopy |
| EIS | electrochemical impedance spectroscopy |
| PD | potentiodynamic polarization |
| SEM | scanning electron microscopy |
| AFM | atomic force microscopy |

## ■ REFERENCES

(1) Tang, Z. A review of corrosion inhibitors for rust preventative fluids. *Curr. Opin. Solid State Mater. Sci.* **2019**, *23*, 100759.
(2) Anh, H. T.; Vu, N. S. H.; Huyen, L. T.; Tran, N. Q.; Thu, H. T.; Bach, L. X.; Trinh, Q. T.; Prabhakar Vattikuti, V. P.; Nam, N. D. Ficus racemosa leaf extract for inhibiting steel corrosion in a hydrochloric acid medium. *Alexandria Eng. J.* **2020**, *59*, 4449−4962.
(3) Alrefaee, S. H.; Rhee, K. Y.; Verma, C.; Quraishi, M. A.; Ebenso, E. E. Challenges and advantages of using plant extract as inhibitors in modern corrosion inhibition systems: Recent advancements. *J. Mol. Liq.* **2021**, *321*, 114666.
(4) Shahini, M. H.; Ramezanzadeh, M.; Bahlakeh, G.; Ramezanzadeh, B. Superior inhibition action of the Mish Gush (MG) leaves extract toward mild steel corrosion in HCl solution: Theoretical and electrochemical studies. *J. Mol. Liq.* **2021**, *332*, 115876.
(5) Shahini, M. H.; Ramezanzadeh, M.; Ramezanzadeh, B. Effective steel alloy surface protection from HCl attacks using Nepeta Pogonesperma plant stems extract. *Colloids Surf., A* **2022**, *634*, 127990.
(6) Trung, D. C.; Pham, T. T.; Minh, Q. B. P.; Panaitescu, C.; Tran, N. Q.; Anh, H. T.; Bach, L. X.; Nguyen Dang, N. D. The use of Piper Betle leaf extract for forming a barrier layer on steel surface in hydrochloric acid solution. *Prog. Org. Coat.* **2021**, *158*, 106340.
(7) Tan, B.; He, J.; Zhang, S.; Xu, C.; Chen, S.; Liu, H.; Li, W. Insight into anti-corrosion nature of Betel leaves water extracts as the novel and eco-friendly inhibitors. *J. Colloid Interface Sci.* **2021**, *585*, 287.
(8) Rajendran, S. Nanoparticle-based corrosion inhibitors and self-assembled monolayers. In *Corrosion Protection and Control Using Nanomaterials*; Woodhead Publishing Series in Metals and Surface Engineering; Woodhead Publishing, 2012; pp 283−303.
(9) Manjunathan, P.; Shanbhag, G. V. Application of tin oxide-based materials in catalysis. In *Tin Oxide Materials: Synthesis, Properties, and Applications*; Metal Oxides; Elsevier, 2020; pp 519−553.
(10) Lee, J.; Kuchibhotla, A.; Banerjee, D.; Berman, D. Silica nanoparticles as copper corrosion inhibitors. *Mater. Res. Express* **2019**, *6*, 0850e3.
(11) Biesinger, M. C.; Payne, B. P.; Grosvenor, A. P.; Lau, L. W. M.; Gerson, A. R.; Smart, R. St.C. Resolving surface chemical states in XPS analysis of first row transition metals, oxides and hydroxides: Cr, Mn, Fe, Co and Ni. *Appl. Surf. Sci.* **2011**, *257*, 2717−2730.
(12) Kaspar, P.; Sobola, D.; Dallaev, R.; Ramazanov, S.; Nebojsa, A.; Rezaee, S.; Grmela, L. Characterization of $Fe_2O_3$ thin film on highly oriented pyrolytic graphite by AFM, Ellipsometry and XPS. *Appl. Surf. Sci.* **2019**, *493*, 673−678.
(13) Rémazeilles, C.; Refait, Ph. On the formation of $\beta$-FeOOH (akaganéite) in chloride-containing environments. *Corros. Sci.* **2007**, *49*, 844−857.
(14) Ghods, P.; Isgor, O. B.; Brown, J. R.; Bensebaa, F.; Kingston, D. XPS depth profiling study on the passive oxide film of carbon steel in saturated calcium hydroxide solution and the effect of chloride on the film properties. *Appl. Surf. Sci.* **2011**, *257*, 4669−4677.
(15) Trinh, Q. T.; Bhola, K.; Amaniampong, P. N.; Jérôme, F.; Mushrif, S. H. Synergistic application of XPS and DFT to investigate metal oxide surface catalysis. *J. Phys. Chem. C* **2018**, *122*, 22397−22406.
(16) Dupin, J.-C.; Gonbeau, D.; Vinatier, P.; Levasseur, A. Systematic XPS studies of metal oxides, hydroxides and peroxides. *Phys. Chem. Chem. Phys.* **2000**, *2*, 1319−1324.
(17) Liu, S.; Gao, S.; Wang, Z.; Fei, T.; Zhang, T. Oxygen vacancy modulation of commercial $SnO_2$ by an organometallic chemistry-assisted strategy for boosting acetone sensing performances. *Sens. Actuators, B* **2019**, *290*, 493−502.
(18) El-Lateef, H. M. A.; Shalabi, K.; Abdelwahed, R. S.; Sobhi, M. G.; Esam, M. B. The novel polythiadiazole polymer and its composite with $\alpha$-$Al(OH)_3$ as inhibitors for steel alloy corrosion in molar $H_2SO_4$: Experimental and computational evaluations. *J. Ind. Eng. Chem.* **2022**, *105*, 238−250.
(19) Alnajjar, A. O.; El-Lateef, H. M. A.; Khalaf, M. M.; Ibrahim, M. A. M. Steel protection in acidified 3.5% NaCl by novel hybrid composite of $CoCrO_3$/polyaniline: Chemical fabrication, physico-chemical properties, and corrosion inhibition performance. *Constr. Build. Mater.* **2022**, *317*, 125918.
(20) Gouda, M.; Khalaf, M. M.; Shalabi, K.; Al-Omair, M. A.; El-Lateef, H. M. A. Synthesis and Characterization of Zn−Organic Frameworks Containing Chitosan as a Low-Cost Inhibitor for Sulfuric-Acid-Induced Steel Corrosion: Practical and Computational Exploration. *Polymers* **2022**, *14*, 228.
(21) Gouda, M.; El-Lateef, H. M. A. Novel Cellulose Derivatives Containing Metal (Cu, Fe, Ni) Oxide Nanoparticles as Eco-Friendly Corrosion Inhibitors for C-Steel in Acidic Chloride Solutions. *Molecules* **2021**, *26*, 7006.
(22) El-Lateef, H. M. A.; Gouda, M.; Khalaf, M. M.; Al-Shuaibi, M. A. A.; Mohamed, I. M. A.; Shalabi, K.; El-Shishtawy, R. M. Experimental and In-Silico Computational Modeling of Cerium Oxide Nanoparticles Functionalized by Gelatin as an Eco-Friendly Anti-Corrosion Barrier on X60 Steel Alloys in Acidic Environments. *Polymers* **2022**, *14*, 2544.
(23) Aslam, R.; Mobin, M.; Shoeb, M.; Parveen, M.; Zehra, S.; Aslam, J. Synthesis, Characterization and Corrosion Inhibition Performance of Glycine-Functionalized Graphene/$Fe_3O_4$ Nanocomposite (Gr/Fe@Gly NC) for Mild Steel Corrosion in 1 M HCl. *Arabian J. Sci. Eng.* **2021**, *46*, 5489−5503.
(24) Khamis, E. A.; Hamdy, A.; Morsi, R. E. Magnetite nanoparticles/polyvinyl pyrrolidone stabilized system for corrosion inhibition of carbon steel. *Egypt. J. Pet.* **2018**, *27*, 919−926.
(25) Nithyadevi, P.; Rathish, R. J.; Bama, J. S.; Rajendran, S.; Joany, R. M.; Pandiarajan, M.; Anandan, A. Inhibition of corrosion of mild steel in well water by $TiO_2$ nanoparticles and an aqueous extract of May flower. *Nanosyst.: Phys., Chem., Math.* **2016**, *7*, 711−723.
(26) Yuan, Z.-Y.; Song, C.; Wang, H.; Zhang, J. EIS Equivalent Circuits. In *Electrochemical Impedance Spectroscopy in PEM Fuel Cells*; Springer: London, 2011; pp 139−192.


https://doi.org/10.1021/acsomega.2c05545
*ACS Omega* 2022, 7, 38061−38068

(27) Hoai Vu, N. S.; Hien, P. V.; Mathesh, M.; Hanh Thu, V. T.; Nam, N. D. Improved Corrosion Resistance of Steel in Ethanol Fuel Blend by Titania Nanoparticles and Aganonerion polymorphum Leaf Extract. *ACS Omega* **2019**, *4*, 146−158.
(28) Mourya, P.; Banerjee, S.; Rastogi, R. B.; Singh, M. M. Inhibition of mild steel corrosion in hydrochloric and sulfuric acid media using a thiosemicarbazone derivative. *Ind. Eng. Chem. Res.* **2013**, *52*, 12733−12747.



https://doi.org/10.1021/acsomega.2c05545
*ACS Omega* 2022, 7, 38061−38068